

Probing the Cosmological Principle in the counts of radio galaxies

Carlos A. P. Bengaly Jr.,^a Roy Maartens,^{a,b} Mario G. Santos^{a,c}

^aDepartment of Physics & Astronomy, University of the Western Cape,
Cape Town 7535, South Africa

^bInstitute of Cosmology & Gravitation, University of Portsmouth,
Portsmouth PO1 3FX, United Kingdom

^cSKA South Africa, The Park, Pinelands 7405, South Africa

E-mail: carlosap87@gmail.com

Abstract. According to the Cosmological Principle, the matter distribution on very large scales should have a kinematic dipole that is aligned with that of the CMB. We determine the dipole anisotropy in the number counts of two all-sky surveys of radio galaxies. For the first time, this analysis is presented for the TGSS survey. This allows us to check consistency of the radio dipole at low and high frequencies by comparing the TGSS results with the well-known NVSS survey. After matching the flux thresholds of the catalogues and adopting a strict masking scheme, we find dipole directions that are in good agreement with each other and with the CMB dipole. In order to compare the amplitude of the dipole with predictions, we produce sets of lognormal realisations, including galaxy clustering and the Poisson noise, and simulated redshift distributions which fit the NVSS and TGSS source counts. The measured dipole is ~ 3 times larger than the predicted signal for NVSS, but for TGSS the dipole is ~ 8 times larger. The anomalously large dipole amplitudes are unlikely to be a cosmological signal, especially since the surveys differ significantly in dipole amplitude while agreeing in direction. It is more likely that the anomaly arises due to low source density, and possible unidentified systematics. More data will be needed in order to clarify this inconsistency.

Contents

1	Introduction	1
2	The observational data	2
3	Estimator, mock data and uncertainties	3
4	Measured dipoles	6
5	Discussion and conclusions	7

1 Introduction

A fundamental hypothesis of the current standard model of cosmology is statistical homogeneity and isotropy, i.e., the absence of privileged positions and directions in the Universe on sufficiently large scales. This is the Cosmological Principle and it applies for fundamental observers, who see no kinematic dipole in the cosmic microwave background (CMB) radiation. Our velocity relative to fundamental observers is deduced from the dipole anisotropy in the CMB temperature, which corresponds to [1, 2]

$$\beta \equiv \frac{v}{c} = 1.23 \times 10^{-3} \quad \text{towards the direction } (l, b) = (264^\circ, 48^\circ) \text{ in galactic coordinates.} \quad (1.1)$$

In the standard cosmological model, this dipole arises from the Doppler boost of CMB photons due to our relative peculiar velocity¹, so that we should observe statistical isotropy once this signal is taken into account. Analyses have been performed using CMB observations and are consistent with isotropy.²

A critical requirement of statistical isotropy is that the Solar System rest frame seen in the CMB and in the number counts of distant radio sources should be consistent. A test of this was proposed in [7], which estimated the dipole amplitude we should see in the projected source distribution, given the velocity inferred from the CMB dipole, and taking into account the Doppler-boosted frequency of sources and the aberration of their locations in the sky. The first implementation of this test was carried out in [8], which combined the Green Bank 1987 (87GB) and Parkes-MIT-NRAO (PMN) catalogues, but due to the limited number of sources ($\sim 40,000$), it was not possible to obtain a statistically significant signature of our velocity. This was obtained by [9], which found a $> 2\sigma$ detection of our relative motion in the NRAO VLA Sky Survey (NVSS), with roughly 5 times more sources. The result was consistent with the CMB dipole within 2σ confidence level (CL) for both amplitude and direction.

The analysis was reassessed in [10], which obtained a similar direction to [9], but the amplitude was consistent with a peculiar velocity of $v \sim 1500$ km/s, i.e., much larger than that seen in the CMB. Moreover, [10] found that this result could not be reproduced at random with $> 99\%$ CL. Other analyses of the NVSS data were performed [11, 12, 13, 14, 15], with most of them confirming the results of [10]. The exceptions were [16, 17], which pointed out that the large radio dipole could be partially ascribed to the local structure, thus reducing the tension between the observed and the expected dipole signal from $\sim 3\sigma$ to $(2.2 - 2.8)\sigma$, depending on the method and the flux cut-off adopted. Some alternative explanations for this result, such as the existence of a large void in the local Universe [18], or super-horizon anisotropic modes from primordial perturbations [19], were tested against observations. However, none of them could reconcile the expected and observed dipole

¹There are alternative interpretations of the CMB dipole as an intrinsic property arising from, e.g., primordial density perturbations [3], or our location near the centre of a void [4].

²Some potential departures from isotropy have been reported, but the statistical significance and possible physical explanation remain open issues [5, 6].

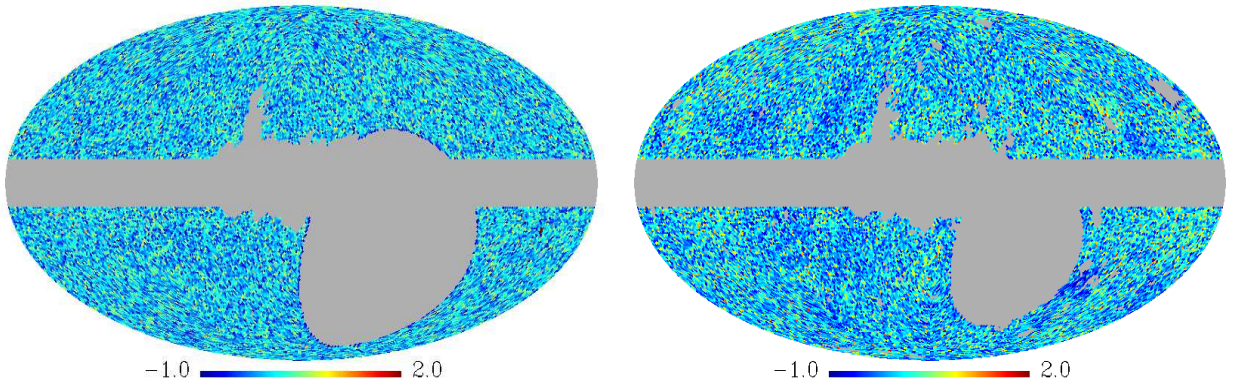


Figure 1. The pixelised number count map of NVSS (left) and TGSS (right) radio sources in the flux ranges $20 < S < 1000$ mJy and $100 < S < 5460$ mJy, respectively. The number counts are normalised to the average count per pixel, and clipped at 2.0 to ease visualisation.

amplitudes unless strong fine-tuning was applied. Other analyses applied to the NVSS catalogue, such as the two-point angular correlation function of its radio sources [20], cross-correlations between NVSS and the WMAP CMB experiment [21], and tests of the isotropy of the slope of the cumulative number source counts [22], on the other hand, revealed no significant departure from the standard cosmological model assumptions.

Here we perform a new assessment of the cosmic radio dipole. Using the new all-sky continuum survey TGSS (TIFR GMRT Sky Survey), we probe for the first time the dipole in a different all-sky survey than NVSS. More importantly, we perform a comparison of the dipoles found at different frequencies, given that TGSS operates at a much lower frequency band than NVSS. We also follow the idea of [17] and test the hypothesis that a large dipole is related to local structure, by simulating sky maps for both surveys, using a simulated redshift distribution and assuming a galaxy bias.

The paper is organised as follows: section 2 describes the observational data and its processing; section 3 discusses the methodology adopted; section 4 presents the results and, finally, our discussion and concluding remarks are given in section 5.

2 The observational data

The radio continuum data here adopted consists of two surveys: NVSS, conducted by the VLA at high frequency, 1.4 GHz [23], and TGSS, conducted by GMRT at low frequency, 150 MHz [24]. Both cover a large area of the sky ($\text{DEC} > -40^\circ$ in NVSS and $\text{DEC} > -53^\circ$ in TGSS), so they are suitable to carry out isotropy tests. In order to compare the number count dipoles, we match their flux ranges using $S \propto \nu^\alpha$, where $\alpha = 0.76$ [25] is the spectral index, so that

$$S_{\text{NVSS}} = S_{\text{TGSS}} \left(\frac{\nu_{\text{TGSS}}}{\nu_{\text{NVSS}}} \right)^\alpha = 0.183 S_{\text{TGSS}}. \quad (2.1)$$

We choose $S_{\text{TGSS}} > 100$ mJ since the TGSS is complete in this range [24], and $S_{\text{NVSS}} < 1000$ mJy in order to remove the brightest sources of this data-set. Hence, a TGSS flux range of $100 < S < 5460$ mJy roughly corresponds to $20 < S < 1000$ mJy in NVSS.

In order to purify the TGSS and NVSS catalogues, we adopt a rigorous masking procedure to deal with well-known contamination. This involves the elimination of pixels in the following regions:

- Close to the galactic plane, i.e., $|b| \leq 10^\circ$.
- Within 1° of the local radio sources given in [26].

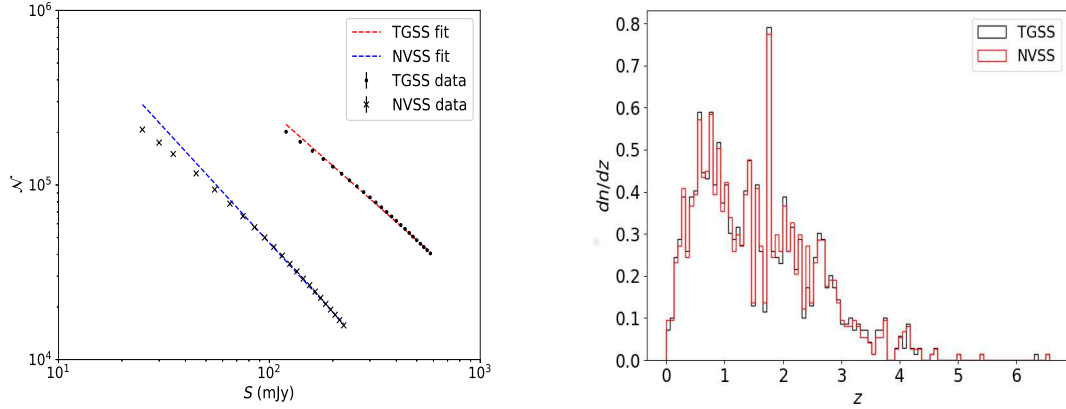


Figure 2. Source counts (3.3) per flux bin per solid angle for TGSS and NVSS data, compared to their best fits (left); normalised redshift distribution dn/dz for both catalogues, based on S^3 simulations (right).

- Within 1° of local superclusters given in Table 1 of [16].
- RMS noise above $S = 1.95$ mJy/beam in TGSS.
- Galactic foreground emission above $T = 50$ K according to the 408 MHz continuum map in [27].

The final TGSS and NVSS maps are shown Fig. 1 for $100 < S_{\text{TGSS}} < 5460$ mJy and $20 < S_{\text{NVSS}} < 1000$ mJy, at a resolution of $N_{\text{side}} = 64$, so that each pixel is $\sim 55'$. The remaining sky area and source numbers after the masking procedure just described are:

$$\text{TGSS} \quad f_{\text{sky}} \simeq 0.69, \quad N_{\text{total}} = 233,598 \quad (2.2)$$

$$\text{NVSS} \quad f_{\text{sky}} \simeq 0.66, \quad N_{\text{total}} = 253,313 \quad (2.3)$$

3 Estimator, mock data and uncertainties

Flux range (mJy)	A_{PN}	SNR
$100 < S_{\text{TGSS}} < 5460$	0.00426	0.9029
$125 < S_{\text{TGSS}} < 5460$	0.00466	0.8500
$150 < S_{\text{TGSS}} < 5460$	0.00502	0.8065
$20 < S_{\text{NVSS}} < 1000$	0.00391	1.0615
$25 < S_{\text{NVSS}} < 1000$	0.00433	0.9955
$30 < S_{\text{NVSS}} < 1000$	0.00470	0.9413

Table 1. The flux range, Poisson noise dipole contribution A_{PN} , and SNR (3.8) for each case. The kinematic dipole amplitude is assumed to be $A_{\text{kin}} = 0.00530$ for NVSS, and $A_{\text{kin}} = 0.00476$ for TGSS, while the predicted LSS dipole amplitude, $A_{\text{LSS}} = 0.00310$, was estimated as explained in the text.

The radio dipole anisotropy is estimated by decomposing the sky into 3072 HEALPix cells ($N_{\text{side}} = 16$), and counting the difference on the number of sources encompassed in opposite hemispheres whose symmetry axes are provided by these cell centres. Therefore, we can construct an estimator, hereafter called the ‘delta-map’, defined by

$$\Delta(\theta) \equiv \frac{\sigma_i^U(\theta) - \sigma_i^D(\theta)}{2\sigma} = A_{\text{obs}} \cos \theta \quad \text{where} \quad \sigma_i^J = \frac{N_i^J}{4\pi(f_{\text{sky}})_i^J}, \quad \sigma = \frac{N_{\text{total}}}{4\pi f_{\text{sky}}}. \quad (3.1)$$

Here $i = 1, \dots, 3072$ labels the hemisphere decomposition, and $J = U, D$ identifies the ‘up’ and ‘down’ hemispheres in this pixelisation scheme; N_i^J , $(f_{\text{sky}})_i^J$, and σ_i^J are the number of sources, the observed sky fraction, and the source density in each hemisphere, respectively, with $N_i^U + N_i^D = N_{\text{total}}$. The angle θ corresponds to the position of the i -th pixel centre in the sky with respect to the estimated direction of our relative motion, and thus the left-hand side of (3.1) provides the dipole amplitude of the source count, A_{obs} , in this direction.

We can compare this quantity with the expected signal due to Doppler and aberration effects [7, 11, 12]:

$$A_{\text{kin}} = [2 + x(1 + \alpha)]\beta, \quad (3.2)$$

where x is the power law index, defined by

$$\mathcal{N} \equiv \frac{dN(> S)}{d\Omega} \propto S^{-x}. \quad (3.3)$$

The plots in the left panel of Fig. 2 show that

$$x \simeq 1.33 \text{ for NVSS}, \quad x \simeq 1.10 \text{ for TGSS}. \quad (3.4)$$

Together with (1.1), this leads to

$$A_{\text{kin}} \simeq 0.00530 \text{ towards the direction } (l, b) = (264^\circ, 48^\circ) \text{ for NVSS}, \quad (3.5)$$

$$A_{\text{kin}} \simeq 0.00476 \text{ towards the direction } (l, b) = (264^\circ, 48^\circ) \text{ for TGSS}, \quad (3.6)$$

This will be hereafter regarded as the expected radio dipole signal if there is consistency with the Cosmological Principle.

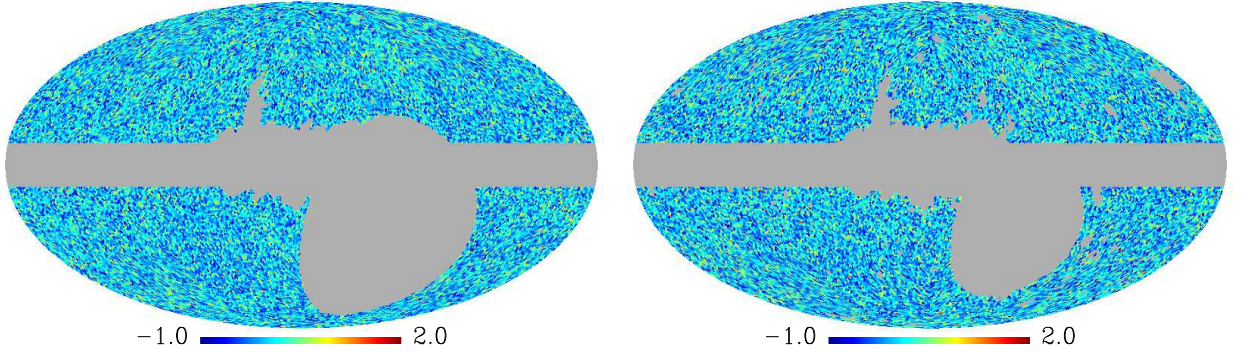


Figure 3. The NVSS (left) and TGSS (right) mock count maps in the same flux range of Fig. 1. Again, the number counts are normalised to the average count per pixel, and clipped at 2.0 to ease visualisation.

The statistical significance of the observed dipole A_{obs} is estimated through 1,000 lognormal realisations of the galaxy density field produced by the FLASK code³ [28]. These mock data-sets assume the angular power spectrum C_ℓ as provided CAMB SOURCES⁴ [29], using the latest *Planck* best-fit Λ CDM as the fiducial cosmology [30]. The power spectrum is computed in five redshift bins with a top-hat window, using the redshift distribution dn/dz shown in the right panel of Fig. 2.

In order to obtain dn/dz , we ran a query on the S³ (SKA Simulated Skies) website⁵ (see [31] for details of the simulation). By assuming a sky area of 11 deg^2 , and the flux range and frequency of both surveys, we obtained 1,048 matches for TGSS and 1,108 for NVSS, as exhibited in the right

³<http://www.astro.iag.usp.br/~flask/>

⁴<http://camb.info/sources/>

⁵http://s-cubed.physics.ox.ac.uk/s3_sex

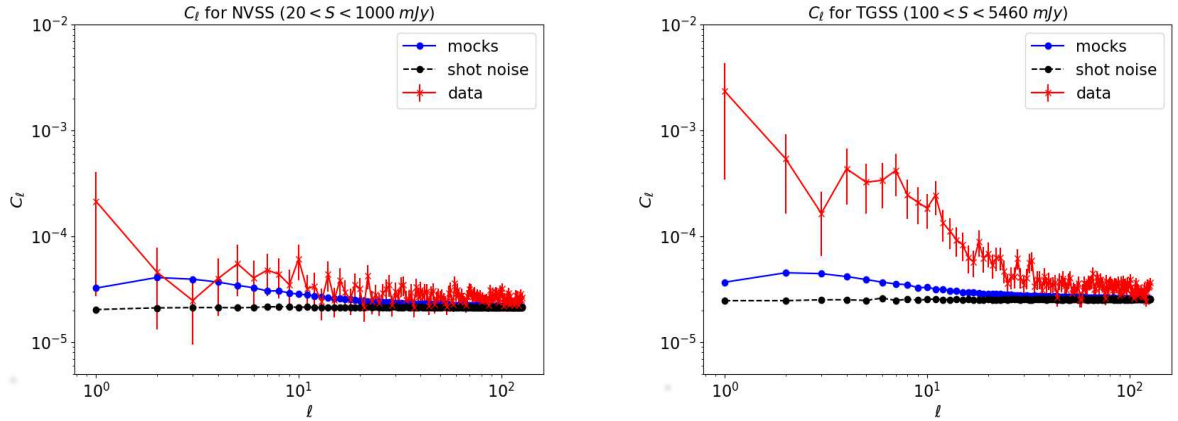


Figure 4. The angular power spectrum, C_ℓ , for the NVSS (left) and TGSS (right) maps featured in Fig. 1. The uncertainties are given by $\sigma_{C_\ell}/C_\ell = \sqrt{2/(2\ell+1)f_{\text{sky}}}$. We also show the average spectra for 1,000 NVSS and TGSS mock catalogues in blue, while the black dots give the shot noise contribution.

panel of Fig. 2. These values correspond to an average source density of $\bar{n} \sim 100$ sources/deg², so that we normalise the source density of the mocks to match both \bar{n} and N_{total} of the real data once we apply their masks, and Poisson-sample the number count fields across the available sky area.

For the galaxy bias, we assume a simple linear model

$$b = 1.6 + 0.7z. \quad (3.7)$$

This choice is similar to the fitting expression given by [17], but without their z^2 contribution.

Finally, we apply a dipolar modulation in the simulated number counts according to (3.5) and (3.6).

As a result of this procedure, we obtain mock NVSS and TGSS catalogues that reproduce the features of the real data, i.e., the shot noise and the galaxy clustering according to the Λ CDM matter density perturbations, the dn/dz in the considered flux range, and their incomplete sky coverage. Examples of the simulated maps that follow from this prescription are shown in Fig. 3.

The statistical significance is estimated by the number of simulated data-sets that can reproduce the observed dipole A_{obs} or larger. If this fraction corresponds to $< 0.5\%$, we will characterise the anisotropy as anomalous. Figure 4 shows the angular power spectra of the real maps, with uncertainties given by cosmic variance, and their shot noise. The average C_ℓ of the mock data-sets are also shown. We imposed a maximum $\ell_{\text{max}} = 128$.

It is clear that the power spectra are indistinguishable from shot noise when $C_\ell \gtrsim 30$ for both surveys. The TGSS data shows much larger number density fluctuations than the NVSS, and than those of the mock data, even when cosmic variance is taken into account. The NVSS power spectrum is only inconsistent with the realisations when $\ell = 10$, although its dipole and octopole are just marginally in agreement with them.

Before proceeding with the delta-map analysis, we can perform a rough assessment of the signal-to-noise ratio (SNR) of the kinematic dipole detection, in a similar fashion to [32] (see also [8]). The SNR is then defined as

$$\text{SNR} = \frac{A_{\text{kin}}^2}{\sqrt{A_{\text{LSS}}^2 + A_{\text{PN}}^2}}, \quad (3.8)$$

where A_{kin} is given by (3.5) and (3.6), while A_{LSS} is obtained from the average C_1 of the 1,000 FLASK

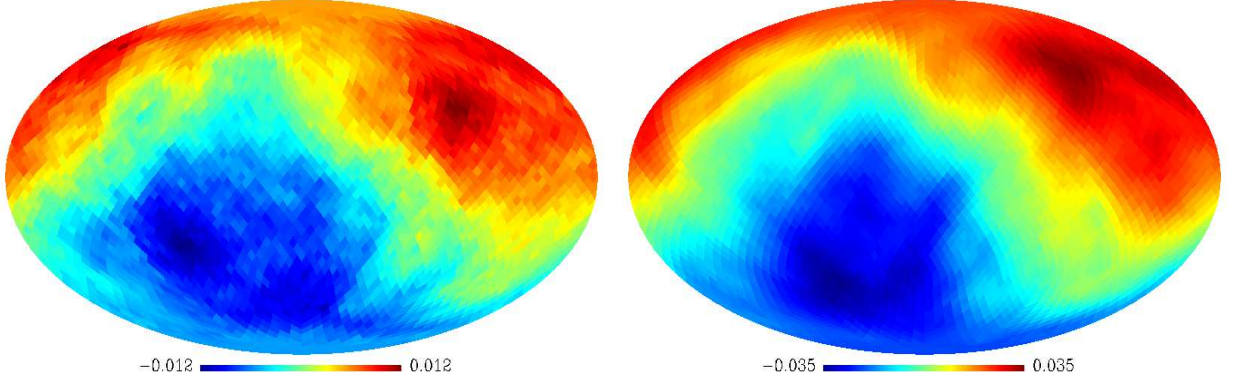


Figure 5. The dipole anisotropy of NVSS (left) and TGSS (right) source counts from applying the delta-map (3.1) to the data shown in Fig. 1.

realisations following the above prescription⁶:

$$A_{\text{LSS}} = \frac{3}{2} \sqrt{\frac{C_1}{\pi}}. \quad (3.9)$$

The Poisson noise contribution to the dipole is given by

$$A_{\text{PN}} = \frac{3}{2} \sqrt{\frac{f_{\text{sky}}}{\pi \bar{n}}}, \quad (3.10)$$

where \bar{n} is the average number of sources per steradian in the unmasked sky area.

The results of the SNR estimate are displayed in Table 1. We note that the Poisson noise contribution, A_{PN} , is comparable to the amplitude of the kinematic dipole A_{kin} , for all cases analysed. Considering also that $A_{\text{LSS}} \simeq 0.0031$, we obtain $\text{SNR} < 1$ for all cases, except for the NVSS catalogue with $20 < S_{\text{NVSS}} < 1000$ – and in this case, the SNR is barely above 1. Because of this, we only consider the largest flux ranges available, in order to minimise the effects from the large shot noise, A_{PN} , as well as the contribution from non-negligible clustering, A_{LSS} .

4 Measured dipoles

Figure 5 shows the delta-map result for the TGSS and NVSS dipoles, while Table 2 compares the previous analyses from the literature with ours. We can see that the dipole directions are quite consistent with the CMB, but the amplitude is much higher than the predicted value in (3.2) for both surveys, especially in the TGSS case.

Our NVSS results agree, within the 1σ uncertainty quoted, with most previous estimates for both dipole amplitude and direction, especially the results of [17]. Our results are also consistent with the analysis of [10], which adopted the same maximum flux cut-off, $S < 1000$ mJy, although the mask was different. Our analysis thus confirms the tension between the CMB and the radio count dipole amplitude that has been previously reported for the NVSS, and extends this tension to the low-frequency TGSS survey, for which the discrepancy is even stronger.

Figure 6 compares the delta-map dipoles measured from the actual data with the dipoles extracted from the mock catalogues. For the latter, we obtained

$$A = 0.0065^{+0.0029}_{-0.0020} \quad \text{at } 95\% \text{ CL}, \quad (4.1)$$

⁶In order to obtain A_{LSS} for the SNR estimate, we did not include Poisson noise or the dipole modulation A_{kin} in the number count maps (unlike the mocks for the C_ℓ shown in Fig. 4). Therefore, the only expected contribution to this average C_1 will come from galaxy clustering.

Survey	Flux range (mJy)	A	(l, b)	ref.
TGSS	$100 < S < 5460$	0.035 ± 0.004	$(243.00^\circ \pm 12.00^\circ, 45.00^\circ \pm 3.00^\circ)$	This work
NVSS	$20 < S < 1000$	0.012 ± 0.004	$(253.12^\circ \pm 11.00^\circ, 27.28^\circ \pm 3.00^\circ)$	This work
NVSS (other work)	$S > 20$	0.021 ± 0.006	$(244.69^\circ \pm 27.00^\circ, 41.18^\circ \pm 29.00^\circ)$	[9]
	$20 < S < 1000$	0.021 ± 0.005	$(252.22^\circ \pm 10.00^\circ, 42.74^\circ \pm 9.00^\circ)$	[10]
	$S > 15$	0.027 ± 0.005	$(213.99^\circ \pm 20.00^\circ, 15.30^\circ \pm 14.00^\circ)$	[11]
	$S > 25$	0.019 ± 0.005	$(248.47^\circ \pm 19.00^\circ, 45.56^\circ \pm 9.00^\circ)$	[12]
	$S > 20$	0.010 ± 0.005	$(256.49^\circ \pm 9.00^\circ, 36.25^\circ \pm 11.00^\circ)$	[13]
	$S > 20$	0.012 ± 0.005	$(253.00^\circ, 32.00^\circ)$	[17]
	$S > 10$	0.019 ± 0.002	$(253.00^\circ \pm 2^\circ, 28.71^\circ \pm 12^\circ)$	[16]

Table 2. The dipole amplitude A and direction (l, b) (galactic coordinates) of the TGSS and NVSS catalogues, as obtained from our delta-map. The error bars on A are given by Poisson noise, whereas the direction uncertainties correspond to the distance to the two nearest pixel coordinates where the maximal dipole power is attained. We also show some results from the literature for the NVSS case for comparison.

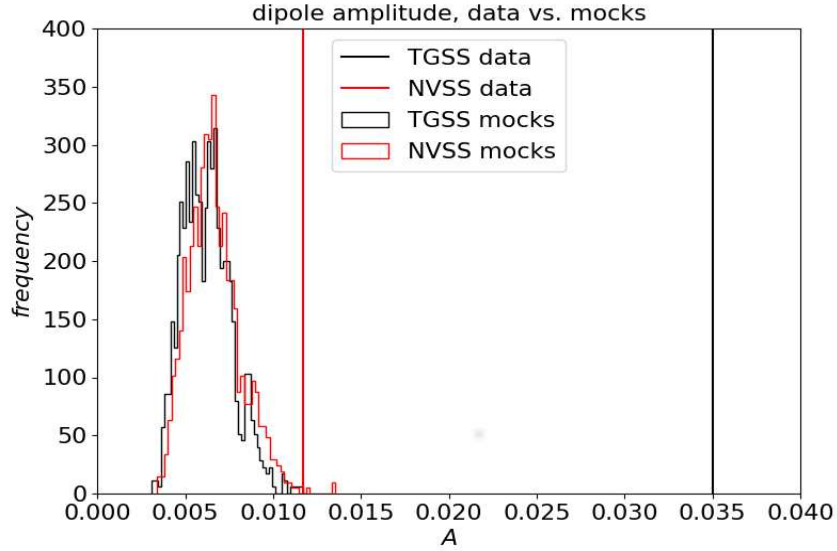


Figure 6. The comparison between the dipole amplitude from NVSS (red) and TGSS (black) real and mock catalogues, as obtained from the delta-map estimator. The vertical lines are the observed values, while the histograms give the results from 1,000 realisations of each catalogue.

where the central value corresponds to the median dipole amplitude. It is apparent that the simulated data-sets perform poorly in reproducing the real data values: no TGSS realisations give $A > A_{\text{obs}}$, whereas only 3 NVSS realisations satisfied this condition, even though we included the galaxy clustering and Poisson noise contributions. The tension in the TGSS case is much stronger than for NVSS. These results may be due to the large shot noise and possible systematics that we could not account for, in both catalogues.

5 Discussion and conclusions

As we can see in Fig. 5 and Table 2, the dipole directions obtained in the two catalogues are indeed very close to the CMB kinematic dipole, i.e., $(l, b) = (264^\circ, 48^\circ)$. This is a striking result, as we

provide another confirmation of the agreement between the CMB and the radio continuum dipole directions, with agreement at low and high radio frequencies. On the other hand, the amplitudes are much higher than the expected value given in (3.2): the NVSS dipole is ~ 3 times larger and the TGSS is ~ 8 times larger. The disagreement between the amplitudes is also an issue.

Other analyses reported similar tension in the NVSS dipole amplitude, and our results are consistent with most of them. It is not possible to explain this tension purely in terms of well-known local contaminants (e.g. low- z bright radio sources, nearby clusters, galactic contamination, regions exhibiting high rms flux noise etc.), since most of them have been taken into account, as in [16]. Since different approaches have been used to probe the radio count dipole, and all of them produce quite similar results, this anomalously large signal is likely to arise from the data and not the methods.

Among all previous analyses, the work of [17] showed that the tension between the estimated and expected NVSS dipole could be somewhat alleviated by taking galaxy clustering into account. We used a different method to include the effects of clustering. We used the FLASK code to produce sets of 1,000 lognormal NVSS and TGSS mocks, based on the Λ CDM angular power spectrum, and on the redshift distribution obtained from the S^3 simulations. We adopted a galaxy bias scaling linearly with redshift and used the same sky coverage as the actual data-sets. As shown in Fig. 6, the mock data is unable to reproduce the observed dipole amplitude A_{obs} for either catalogue at 99% CL.

Our results do not agree with theoretical expectations for the amplitude of the number count dipole even after removing local contaminants and taking galaxy clustering into account. The current all-sky radio catalogues present a dipole anisotropy with anomalous amplitude, and with a disagreement in magnitudes. This is very unlikely to be a signal of a violation the Cosmological Principle. It is more likely that the number density and depth of these surveys are not sufficient for an accurate determination of the dipole amplitude. Both data-sets are noisy, as shown in Table 1: the Poisson noise A_{PN} values are of the same order as the expected signal A_{kin} . In addition, there are potentially unidentified systematics in the data-sets that may directly affect the number counts, especially in the TGSS, given the difficulty of flux calibration when observing at 150 MHz. Future SKA surveys will have the number density to make a high signal-to-noise measurement of the dipole direction and amplitude [33, 34, 35], allowing us to test the Cosmological Principle with confidence.

Acknowledgements:

We thank Song Chen and Subir Sarkar for useful comments. The authors were supported by the South African SKA Project. RM was also supported by the UK STFC, Grant ST/N000668/1. Some of our results made use of the HEALpix package.

References

- [1] Kogut, A. *et al.*, *Dipole Anisotropy in the COBE Differential Microwave Radiometers First-Year Sky Maps*. *ApJ* **419** (1993) 1
- [2] Aghanim, N. *et al.*, *Planck 2013 results. XXVII. Doppler boosting of the CMB: Eppure si muove*. *A & A* **571** (2014) A27
- [3] Roldan, O., Notari, A. & Quartin, M., *Interpreting the CMB aberration and Doppler measurements: boost or intrinsic dipole?* *JCAP* **1606** (2016) 026
- [4] Cusin, G. *et al.*, *Are we living near the center of a local void?* *JCAP* **1703** (2017) 038
- [5] Schwarz, D. J. *et al.*, *CMB Anomalies after Planck*. *Class. Quant. Grav.* **33** (2016) 184001
- [6] Ade, P. A. R. *et al.*, *Planck 2015 results. XVI. Isotropy and statistics of the CMB*. *A & A* **594** (2016) A16
- [7] Ellis, G. F. R. & Baldwin, J. E., *On the expected anisotropy of radio source counts*. *MNRAS* **206** (1984) 377
- [8] Baleisis, A. *et al.*, *Searching for large scale structure in deep radio surveys*. *MNRAS* **297** (1998) 545
- [9] Blake, C. & Wall, J. W., *A velocity dipole in the distribution of radio galaxies*. *Nature* **416** (2002) 150
- [10] Singal, A. K., *Large peculiar motion of the solar system from the dipole anisotropy in sky brightness due to distant radio sources*. *ApJ* **742** (2011) L23
- [11] Gibelyou, C. & Huterer, D., *Dipoles in the sky*. *MNRAS* **427** (2012) 1994
- [12] Rubart, M. & Schwarz, D. J., *Cosmic radio dipole from NVSS and WENSS*. *A & A* **555** (2013) A117
- [13] Tiwari, P. *et al.*, *Dipole anisotropy in sky brightness and source count distribution in radio NVSS data*. *Astropart. Phys.* **61** (2014) 1
- [14] Fernández-Cobos, F. *et al.*, *Searching for a dipole modulation in the large-scale structure of the Universe* *MNRAS* **441** (2014) 2392
- [15] Tiwari, P. & Jain, P., *Dipole Anisotropy in Integrated Linearly Polarized Flux Density in NVSS Data*. *MNRAS* **447** (2015) 2658
- [16] Colin, J. *et al.*, *High-redshift radio galaxies and divergence from the CMB dipole*. *MNRAS* **471** (2017) 1045
- [17] Tiwari, P. & Nusser, A., *Revisiting the NVSS number count dipole*. *JCAP* **1603** (2016) 062
- [18] Rubart, M., Bacon, D. & Schwarz, D. J., *Impact of local structure on the cosmic radio dipole*. *A & A* **565** (2014) A111
- [19] Ghosh, S., *Generating Intrinsic Dipole Anisotropy in the Large Scale Structures*. *PRD* **89** (2014) 063518
- [20] Chen, S. & Schwarz, D. J., *Angular two-point correlation of NVSS galaxies revisited*. *A & A* **591** (2016) A135
- [21] Hernandez-Monteagudo, C., *Revisiting the WMAP - NVSS angular cross correlation. A skeptic view*. *A & A* **520** (2010) A101
- [22] Ghosh, S. & Jain, P., *Testing the Isotropy of the log N-log S Slope for the NVSS Radio Catalog*. *ApJ* **843** (2017), 13
- [23] Condon, J. J. *et al.*, *The NRAO VLA Sky survey*. *AJ* **115** (1998) 1693
- [24] Intema, H. T. *et al.*, *The GMRT 150 MHz All-sky Radio Survey: First Alternative Data Release TGSS ADR1*. *A & A* **598** (2017) A78
- [25] Tiwari, P., *Radio spectral index from NVSS and TGSS*. arXiv:1609.01308
- [26] Van Velzen, S. *et al.*, *Radio galaxies of the local universe: all-sky catalog, luminosity functions, and clustering*. *A & A* **544** (2012) A18
- [27] Haslam, C. G. T. *et al.*, *A 408 MHz all-sky continuum survey. II. The atlas of contour maps*. *A & A* **SS 47** (1982) 1

- [28] Xavier, H. S., Abdalla, F. B. & Joachimi, B., *Improving lognormal models for cosmological fields.* *MNRAS* **459** (2016) 3693
- [29] Challinor, A. & Lewis, A., *The linear power spectrum of observed source number counts.* *PRD* **84** (2011) 043516
- [30] Ade, P.A.R. *et al.*, *Planck 2015 results. XIII. Cosmological parameters.* *A & A* **594** (2016) A13
- [31] Wilman, R. J. *et al.*, *A semi-empirical simulation of the extragalactic radio continuum sky for next generation radio telescopes.* *MNRAS* **388** (2008) 1335
- [32] Itoh, Y., Yahata, K. & Takada, M., *A dipole anisotropy of galaxy distribution: Does the CMB rest-frame exist in the local universe?* *PRD* **82** (2010) 043530
- [33] Crawford, F., *Detecting the cosmic dipole anisotropy in large-scale radio surveys.* *ApJ* **692** (2009) 887
- [34] Schwarz, D. J. *et al.*, *Testing foundations of modern cosmology with SKA all-sky surveys.* *PoS AASKA* **14** (2015) 032
- [35] Maartens, R., Clarkson, C. & Chen, S., *The kinematic dipole in galaxy redshift surveys.* arXiv:1709.04165